



**HAL**  
open science

## Design and Experimental Validation of a Ducted Counter-rotating Axial-flow Fans System

Hussain Nouri, Florent Ravelet, Farid Bakir, Christophe Sarraf

► **To cite this version:**

Hussain Nouri, Florent Ravelet, Farid Bakir, Christophe Sarraf. Design and Experimental Validation of a Ducted Counter-rotating Axial-flow Fans System. 2012. hal-00705797v1

**HAL Id: hal-00705797**

**<https://hal.science/hal-00705797v1>**

Preprint submitted on 8 Jun 2012 (v1), last revised 28 Aug 2012 (v2)

**HAL** is a multi-disciplinary open access archive for the deposit and dissemination of scientific research documents, whether they are published or not. The documents may come from teaching and research institutions in France or abroad, or from public or private research centers.

L'archive ouverte pluridisciplinaire **HAL**, est destinée au dépôt et à la diffusion de documents scientifiques de niveau recherche, publiés ou non, émanant des établissements d'enseignement et de recherche français ou étrangers, des laboratoires publics ou privés.

# Design and Experimental Validation of a Ducted Counter-rotating Axial-flow Fans System

H. Nouri, F. Ravelet,<sup>a)</sup> F. Bakir, and C. Sarraf

*Arts et Metiers ParisTech, DynFluid, 151 boulevard de l'Hôpital, 75013 Paris, France.*

An experimental study on counter-rotating axial-flow fans was carried out. The fans of diameter  $D = 375$  mm were designed using an inverse method. In particular, the system is designed to have a pure axial discharge flow. The counter-rotating fans operate in a ducted-flow configuration and the overall performances are measured in a normalized test bench. The rotation rate of each fan is independently controlled. The axial spacing between the fans can vary from 10 to 150 mm. The results show that the efficiency is strongly increased compared to a conventional rotor or to a rotor-stator stage. The effects of varying the rotation rates ratio on the overall performances are studied and show that the system has a very flexible use, with a large patch of high efficient operating points in the parameter space. Measurements of wall pressure fluctuations in between the two rotors are also performed. They give hints on the overall machine noise and on the flow structure. For small axial spacings there is a strong interaction between the front rotor wake and the rear rotor induced flow that lead to very rich spectra and high levels for the casing pressure fluctuations. The increase of axial spacing from 10 to 150 mm causes only a small decrease of the efficiency and strongly modifies the shape of the spectra and the azimuthal correlations of the pressure fluctuations.

## I. INTRODUCTION

Early studied in the 1930's<sup>1,2</sup>, the counter-rotating machines arouse a greater interest in the turbomachinery field, particularly for their potential improvement of the efficiency with respect to conventional machines by recovering more kinetic energy from the front rotor exit-flow<sup>3-6</sup>. The first counter-rotating machines have appeared in aeronautic and marine applications, in open configuration. Nowadays, these machines with two coaxial axial-flow fans that rotate in opposite direction see a revival of interest in several distinct configurations —open and ducted flows, shrouded or not shrouded rotors— in various subsonic regime applications<sup>7-9</sup>.

All previous studies concluded that the presence of the rear rotor improves the global efficiency<sup>3,4</sup> and also increases the operating flow-rate range. The counter-rotating systems (CRS) moreover allow to reduce the fans radial compactness<sup>6,8</sup>. A CRS requires more axial spacing compared to one simple fan, but not much more than a rotor-stator stage. Another interesting feature of CRS is that it makes it possible to design axial-flow fans with very low angular specific speed  $\Omega = \frac{\omega\sqrt{Q}}{(\Delta p_t/\rho)^{3/4}}$  with  $\omega$  the mean angular velocity,  $Q$  the flow rate,  $\Delta p_t$  the total pressure rise and  $\rho$  the fluid density.

With such advantages (radial compactness and efficiency improvement), the CRS becomes a very interesting solution and the interactions between the rotors needs to be better understood in order to design highly efficient CRS.

The general aim of the present study on ducted counter-rotating axial-flow fans in subsonic regime is to find out a design method for CRS by investigating the

global and the local performances and the interactions between the two rotors. We first present in § II the method that has been used to design the front and the rear rotors. The experimental set-up is presented in § III. Then we report on the overall performances of the system in § IV. The counter-rotating system in its default configuration is studied in § IV A and the effects of varying the rotation ratio and the axial spacing between the rotors are presented in § IV B. The power spectra and the correlation of the wall pressure fluctuations for two axial distances ( $S=10$  mm and  $S=150$  mm) are then studied and discussed in § V. We then give some conclusive remarks in § VI.

## II. DESIGN OF THE ROTORS

The design of the rotors is based on the use of the software MFT (Mixed Flow Turbomachinery) developed by the DynFluid Laboratory<sup>10</sup> to which an original method has been added specifically for the design of the Rear Rotor of the counter-rotating system.

The design point of the CRS is given in Tab. I. The system is designed to achieve a total-pressure rise  $\Delta p_t = 420$  Pa at flow-rate  $Q = 1$  m<sup>3</sup>.s<sup>-1</sup> for a mean rotation rate around 1900 rpm. That would correspond to a angular specific speed  $\Omega \simeq 2.46$  which is a far too low value for an axial machine. The dimensions of the system, the number of blades of the front rotor (FR) and of the rear rotor (RR) and their rotation rates are then imposed. In particular, the number of blades of each rotor was chosen in order to prevent to have the same blade passing frequency or harmonics for both rotors in the lower frequencies range. The system that is presented here has moreover been designed to have a pure axial exit-flow.

An iterative procedure is then performed. The pressure rise of the front rotor is initially chosen and FR is

---

<sup>a)</sup>Electronic mail: florent.ravelet@ensta.org

designed and quickly analysed as explained in § II A. An estimate of the pressure rise that RR would make is then performed (see § II B), based on this analysis. If the total pressure rise of the CRS is not met, the design pressure rise of FR is varied and the calculus are made again. The drawback of this method is that the losses and interactions in-between the two rotors are not taken into account. The effect of the axial spacing  $S$  in particular is not taken into account and some aspects of axial spacing are studied in the present Article.

### A. Design of the Front Rotor

The front rotor was designed with MFT as a conventional fan that meets the specifications reported in Tab. I. The design is based on the inverse method with simplified radial equilibrium<sup>10</sup>.

From the specified total pressure rise, volume flow-rate and rotating speed, optimal values of the radii  $R_{tip}$  and  $R_{hub}$  are first proposed. In a second step, the tip and the hub radii as well as the radial distribution of the circumferential component of the velocity at the rotor outlet,  $C_{u2}(r)$ , could be changed by the user. The available vortex models are the free vortex ( $C_{u2}(r) = \frac{K}{r}$ ), the constant vortex ( $C_{u2}(r) = K'$ ) and the forced vortex ( $C_{u2}(r) = r \cdot K''$ ). In the present case,  $R_{tip} = 187.5 \text{ mm}$ ,  $\frac{R_{hub}}{R_{tip}} = 0.293$  and the vortex model is a constant vortex model. The velocity triangles are then computed for 11 radial sections, based on the Euler equation for perfect fluid with a rough estimate of the efficiency of  $\eta_{est} = 60\%$  and on the equation of simplified radial equilibrium (radial momentum conservation). The blades can then be defined by the local resolution of an inverse problem considering a two-dimensional flow and searching for the best suited cascade to the proposed velocity triangles. The blades are built-up with circular-arc camber lines, with NACA-65 profiles clipped at 0.95 x/c. The blade cascade is defined by the following parameters:  $\gamma$  the stagger angle,  $\sigma$  the solidity,  $c$  the chord length,  $e\%$  the relative thickness and  $C_{z\infty 0}$  the camber coefficient. All have to be computed in order to completely define the geometry of the blade cascade. This inverse problem is solved with the following empirical equations that have been validated for NACA-65 cascades<sup>10</sup>, for  $0.5 \leq \sigma \leq 1.5$  and  $0 \leq C_{z\infty 0} \leq 2.7$ :

$$\gamma = \beta_1 - a, \quad (1)$$

$a$  is the angle of attack and is obtained by:

$$a = \frac{\Delta\beta + 0.94}{q(\beta_1)} + 2.07 \quad (2)$$

with  $q(\beta_1)$  defined by:

$$q(\beta_1) = 2.103 - 4.01910^{-7}\beta_1^{3.382} \quad (3)$$

The solidity  $\sigma$  is computed by:

$$\sigma^{-1} = \left( \mathcal{D} - 1 + \frac{C_2}{C_1} \right) \times \left( \frac{2C_1}{|\Delta C_u|} \right) \quad (4)$$

with  $\mathcal{D}$  the Lieblein's diffusion factor<sup>11</sup> which has an important influence on the performances: the best compromise between losses due to friction and due to blade wake is obtained for  $\mathcal{D}$  around 0.5. According to<sup>11</sup>, this diffusion factor must be between 0.4 and 0.65. The solidity is thus computed at the hub and at the tip. Then equation 5 is used to obtain the chord lengths at the hub and at the tip:

$$c = \sigma \frac{2\pi R}{Z} \quad (5)$$

where  $Z$  is the number of blades. The chord is computed at the tip and at the hub then the intermediate chords are obtained by linearization. Finally, the camber coefficients  $C_{z\infty 0}$  are computed by:

$$C_{z\infty 0} = \frac{a + 2.525}{p(\sigma)} - 0.823 \quad (6)$$

where

$$p(\sigma) = 15.535 - 12.467e^{-0.4242\sigma} \quad (7)$$

The behaviour of the designed machine resulting from the above method can then be analysed using a direct method in order to answer the following questions:

- Is the design-point achieved ?
- What are the characteristics of the machine at the neighbourhood of the design point ?

For the imposed speed of rotation, the direct method rules are applied in order to determine the velocity triangles corresponding to each flow discharge. The effects due to real fluid are taken partially into account with the introduction of an axial-velocity distribution which considers the boundary layers at the hub and casing. Thus, we can obtain the characteristics of the machine in the vicinity of the design-point discharge. If the design point is not met, the blade cascade can be slightly modified by hand, for instance by changing the value of the hub and tip Lieblein's diffusion factors or the number of blades.

In the present case, this direct analysis predicts a mean absolute tangential velocity at the design flow-rate  $C_{u2FR} \simeq 9.6 \text{ m.s}^{-1}$  with a radial distribution uniform within  $\pm 5\%$  (constant vortex design). The Reynolds number based on the inlet relative velocity varies from  $0.6 \times 10^5$  at the hub to  $3 \times 10^5$  at mid-span and  $7 \times 10^5$  at the tip.

TABLE I. Design point of the counter-rotating system for air at  $\rho = 1.21 \text{ kg.m}^{-3}$ 

	CRS	Front Rotor	Rear Rotor
$D$ (mm)	380	380	380
$R_{tip}$ (mm)	187.5	187.5	187.5
$R_{hub}$ (mm)	55	55	55
$Z$	-	11	7
$\Delta p_t$ (Pa)	420	260	160
$N$ (RPM)	1900	2000	1800
$Q$ ( $\text{m}^3.\text{s}^{-1}$ )	1	1	-
$\Omega$	2.46	3.71	-
Other constraints	Axial exit-flow	Constant vortex	-

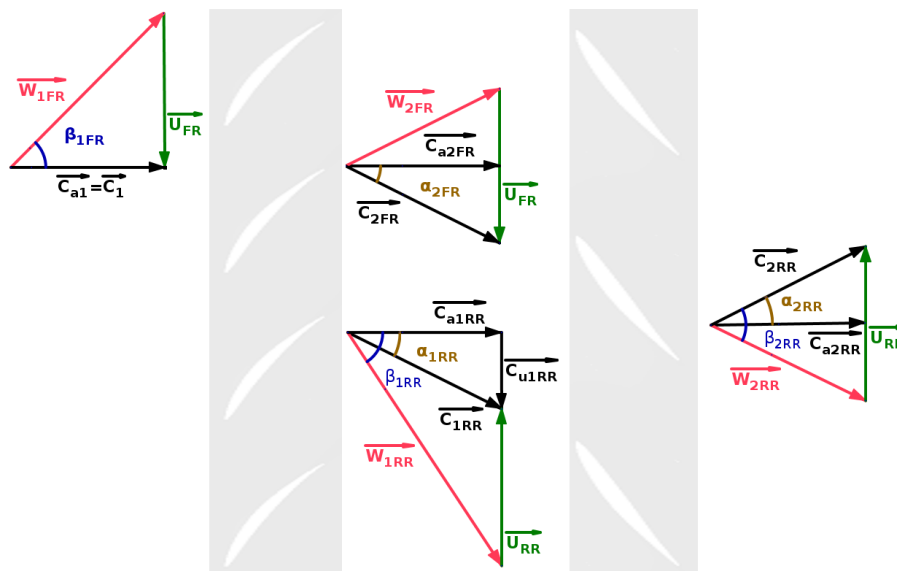


FIG. 1. Velocity Triangles for the CRS. The fluid is flowing from left to right. Please see the Nomenclature for the meaning of the capital letters and subscripts. Please also note that this is a general case where the exit-flow is not constrained to be solely axial

## B. Design of the Rear Rotor

The method used for the design of the rear rotor (RR) is to consider the velocity and the flow angle at the trailing edge of the FR blades. Therefore, FR was analysed with MFT to retrieve the axial and tangential velocities ( $C_{a2FR} = C_{a1RR}$  and  $C_{u2FR} = C_{u1RR}$  respectively) and the angle  $\alpha_{2R1}$  in the absolute reference frame, at the exit along the blade as shown in Fig. 1.

Using a Matlab script and following an iterative procedure, the RR is drawn in such a way that the exit flow is purely axial, that is  $\alpha_{2RR} = 0^\circ$ . The second hypothesis is that the axial velocity profile is kept constant across RR, *i.e.*  $C_{a2RR}(r) = C_{a1RR}(r)$ . Under these assumptions, the total pressure rise of RR should be  $\Delta p_{tRR} =$

$\eta_{est} \rho U_{mRR} C_{u2FR} \simeq 0.6 \times 1.2 \times 22.9 \times 9.6 \simeq 160 \text{ Pa}$ . The blade cascade that lead to the desired velocity triangles is then designed with the previously described inverse method, adjusting the free parameters in such a way that the solidity lays in the range  $0.5 \leq \sigma \leq 1.5$  and that the camber lays in the range  $0 \leq C_{z\infty 0} \leq 2.7$ . After several iterations, the RR was drawn with  $Z = 7$ ,  $\mathcal{D}_{hub} = 0.61$  and  $\mathcal{D}_{tip} = 0.46$ .

The geometrical characteristics of the rotor blades obtained with this method are summarized in Tab. II. Pictures of the Front and Rear rotors are given in Fig. 2.

TABLE II. Blade cascade parameters for the two rotors. Radius  $R$  (mm). Chord length  $c$  (mm). Cascade solidity  $\sigma$ . Stagger angle  $\gamma$  ( $^\circ$ ). Profile designation according to the nomenclature given in Ref.<sup>10</sup>: NACA65(xx)yy with (xx) representing the relative camber and yy standing for the relative thickness. Lieblein’s diffusion factor  $\mathcal{D}$

Radial position	$R$	$c$	$\sigma$	$\gamma$	profile	$\mathcal{D}$
Front Rotor (blade thickness 4.5 mm)						
Hub	55	40.3	1.28	23	NACA 65(26)11	0.62
Mid-span	121.25	58.0	0.84	57	NACA 65(12)07	
Tip	187.5	75.7	0.71	69	NACA 65(07)06	0.44
Rear Rotor (blade thickness 6 mm)						
Hub	55	58.8	1.18	73	NACA 65(03)10	0.61
Mid-span	121.25	72.9	0.66	65	NACA 65(05)08	
Tip	187.5	87.1	0.51	75	NACA 65(04)07	0.46



FIG. 2. Picture of the front rotor (left) and Rear Rotor (right)

### III. EXPERIMENTAL SET-UP

#### A. Test bench

The counter-rotating system is studied in a ducted-flow test rig —AERO<sup>2</sup>FANS— that has been built according to the ISO-5801 standards (installation of category B)<sup>12,13</sup>. The Figure 3 shows this test rig. It consists of a cylindrical pipe of inner diameter  $D = 380$  mm. A bell mouth is flush-mounted at the inlet of the duct to reduce the energy loss due to fluid friction and flow separation of the inlet flow. The upstream face of FR is at a distance  $5D$  from the pipe inlet. A honeycomb is placed upstream of FR to homogenize the incoming flow. Two brushless PANASONIC A4 motors drive each rotor separately and are hidden in a casing of diameter  $0.33D$  and of length  $0.45D$ , with a warhead-shape end. The front and the rear motors are bound to the tube by two rod rows (3 and 5 rods, the first row being at  $0.1D$  from the rear rotor). For the front motor the honeycomb is placed between the two rows to reduce the rods effect on the incoming flow at the inlet of the FR. An anti-gyration device made

of eight metal sheets of thickness 1.5 mm and length  $2D$  is placed  $2D$  downstream of the CRS. It prevents the outgoing flow from having any rotating component by converting the dynamic pressure of the rotational component to thermal energy. Therefore, as the outgoing flow is supposed to contain only axial component, perpendicular to the pressure taps, the static pressure evaluated downstream is more reliable. The static pressure of the axial fan is measured  $1D$  downstream of the anti-rotation device, with an average over four flush-mounted pressure taps. To make the installation more compact, a tube bend of  $180^\circ$  is placed  $1D$  downstream of the pressure taps. The flow rate is measured with a normalized diaphragm, located  $10D$  downstream of the tube bend and  $5D$  upstream of the pipe outlet. The diaphragm has a diameter of  $0.73D$ . An iris damper —originally used for air flow regulation in ducts— is placed at the exit of the pipe to vary the test-bench hydraulic impedance and thereby to vary the operating point of the studied axial-flow fan. Finally, an axial blower can also be used at the exit of the pipe to widen the explored flow-rate.

#### B. Measurements methodology

The study focuses on the influence of the gap between the rotors (axial spacing  $S$ ) as well as on the influence of the speed ratio  $\theta = \frac{N_{FR}}{N_{RR}}$ . Five axial spacings, from  $S = 10$  mm to  $S = 150$  mm were investigated. Clear Plexiglas blocks of different thickness are used to change the axial spacing. The reason of using transparent material is to allow forthcoming optical measurements of the velocity field with Laser Doppler Anemometry (LDA) or Particle Image Velocimetry (PIV). Unless specified the default axial spacing is  $S = 10$  mm. Regarding the speed ratio, each rotor is driven separately so all combinations are possible. The default configuration is  $\theta = 0.9$  (see Tab. I).



TABLE III. Nominal points of FR rotating alone at  $N_{FR} = 2000$  rpm, RR rotating alone at  $N_{RR} = 1800$  rpm and CRS at  $N_{FR} = 2000$  rpm and  $\theta = 0.9$  (see also Fig. 4)

	Front Rotor	Rear Rotor	CRS
Maximum efficiency (%)	45.28	54.48	64.73
nominal $Q$ ( $\text{m}^3 \cdot \text{s}^{-1}$ )	1.03	0.71	0.99
$\Delta p_s$ (Pa)	145.33	88.52	335

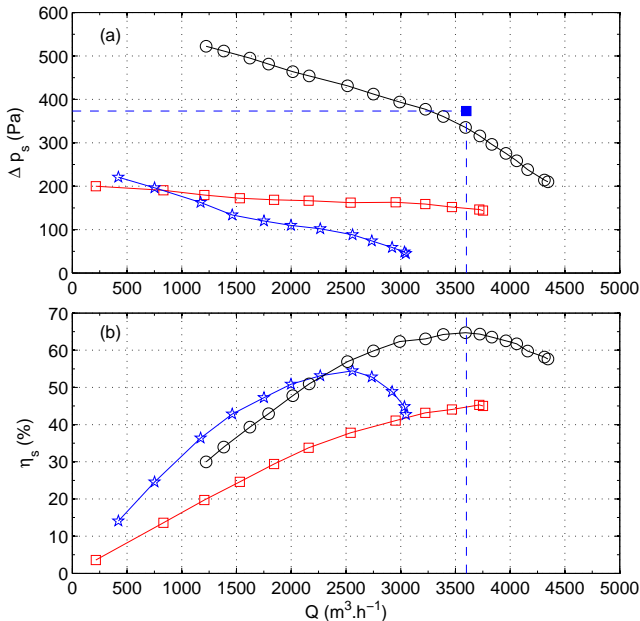


FIG. 4. Fans characteristics: (a) static pressure rise  $\Delta p_s$  vs flow rate  $Q$ ; (b) static efficiency  $\eta_s$  vs flow rate  $Q$ . The axial spacing is  $S = 10$  mm. Red  $\square$ : FR rotating alone at  $N_{FR} = 2000$  rpm (RR has been removed), blue  $\star$ : RR rotating alone at  $N_{RR} = 1800$  rpm (FR has been removed) and black  $\circ$ : CRS at  $N_{FR} = 2000$  rpm and  $\theta = 0.9$ . The blue  $\blacksquare$  and the dashed lines stand for the design point of the CRS

The front rotor rotating alone has a very flat curve (red  $\square$  in Fig. 4). The characteristic curve could not be explored for flow-rates higher than  $3800 \text{ m}^3 \cdot \text{h}^{-1}$ , *i.e.*  $1.06 \text{ m}^3 \cdot \text{s}^{-1}$ , even with the help of the blower. The nominal flow-rate of FR is slightly greater than the design point—it is 3% greater. The measured static pressure rise at the design point is 145.33 Pa, with a relatively low static efficiency of 45%. This is not surprising with no shroud and a large radial gap of 2.5 mm, that is 1.88% relatively to the blade height. Numerical analysis performed with MFT<sup>10</sup> and with Fluent 6.3 give very similar results for the static pressure rise ( $142 \leq \Delta p_s \leq 153$  Pa). The total pressure rise predicted by these two different numerical methods—a model using semi-empirical correlations vs Computational Fluid Dynamics—is roughly

260 Pa. The predicted global performances of FR can thus be considered as validated. The remaining question is about the prediction of the exit-flow velocity components, *i.e.* of the exit-flow angles. This question could of course only be answered with systematic and deep velocity measurements that are scheduled. However, the present global measurements could give partial informations.

The rear rotor rotating alone has a steeper curve (blue  $\star$  in Fig. 4) and its nominal flow-rate  $Q \simeq 2600 \text{ m}^3 \cdot \text{h}^{-1}$  is lower than the design flow-rate of FR and CRS. This is consistent with the bigger stagger angle of the blades (see Tab. II).

Let us examine the velocity triangles in Fig. 1 and consider the case with the front coupled to the rear rotor: the incoming velocity  $C_{1RR} = C_{2FR}$  has an axial component as well as a tangential component. Hence, the flow angle in the relative reference frame reads:

$$\tan(\beta_{1RR}) = \frac{U_{RR} + C_{u1RR}}{C_{a1RR}} \quad (9)$$

Let us consider now the case without the front rotor and assume that the flow through the honeycomb is axial. Since the tangential component does not exist any more and the incoming velocity has only the axial component, equation 9 becomes:

$$\tan(\beta_{1RR}) = \frac{U_{RR}}{C_{a1RR}} \quad (10)$$

Let us now compute the result of equation 9 for the mean radius and at the nominal flow-rate of the CRS, assuming that the tangential velocity is well predicted by MFT, that is  $\langle U_{RR} \rangle \simeq 22.9 \text{ m} \cdot \text{s}^{-1}$ ,  $\langle C_{a1RR} \rangle \simeq 8.8 \text{ m} \cdot \text{s}^{-1}$  and  $\langle C_{u1RR} \rangle = \langle C_{u2FR} \rangle \simeq 9.6 \text{ m} \cdot \text{s}^{-1}$ . This leads to  $\langle \tan(\beta_{1RR}) \rangle \simeq 3.69$ . If we now suppose that RR rotating alone has its maximum efficiency when the tangent of the inlet flow-angle is equal to this value, equation 10 implies that this is for a flow-rate such that  $\langle C_{a1RR} \rangle = \frac{\langle U_{RR} \rangle}{\tan(\langle \beta_{1RR} \rangle)} \simeq 6.2 \text{ m} \cdot \text{s}^{-1}$ , *i.e.*  $Q \simeq 0.705 \text{ m}^3 \cdot \text{s}^{-1}$  or  $2540 \text{ m}^3 \cdot \text{h}^{-1}$ . This is exactly the nominal flow-rate of RR rotating alone (see Fig. 4 and Tab. III). The estimations of the angles behind the front rotor using the direct analysis of MFT thus seem consistent.

The characteristic curve of the CRS (black  $\circ$  in Fig. 4) is steeper than the characteristic curve of FR. It is

roughly parallel to the RR curve. The nominal flow-rate of the CRS matches well with the design flow-rate, *i.e.*  $1 \text{ m}^3 \cdot \text{s}^{-1}$ . The static pressure rise at the nominal discharge ( $\Delta p_{sCRS} = 335 \text{ Pa}$ ) is 10.2% lower than the design point (373 Pa), which is not so bad in view of the rough approximations used to design the system. Please notice that the pressure rise of the CRS is not equal to the addition the pressure rise of the FR with the pressure rise of the RR. The CRS therefore could not be considered as two fans in series and that is because of the very short axial spacing. The question is how the front and the rear rotors interact when operating together? Another open question is how the pressure rise made by the CRS is distributed between each rotor? Does the FR behaves in the same way with or without the RR? Experimental local study or a validated CFD simulation on the rotors interaction could clarify these questions

The CRS has a high static efficiency ( $\eta_{sCRS} = 65\%$ ) compared to a conventional axial-flow fan or to a rotor-stator stage with similar dimensions, working at such Reynolds numbers<sup>14,15</sup>. The gain in efficiency with respect to the front rotor is 20 points, whilst an order of magnitude of the maximum gain using a stator is typically 10 points<sup>14,15</sup>.

Awaiting for more accurate local measurements of the flow angle at the exit of the CRS, a simple test of flow visualization with threads or tufts affixed downstream of the CRS was performed. It has been observed that without the RR the flow is very turbulent. When the RR is operating, at the design configuration ( $\theta = 0.9$  and  $N_{FR} = 2000 \text{ rpm}$ ), the flow is less turbulent, the tufts are oriented with a small angle at the exit. This small angle seems, however to decrease when  $\theta$  is increased between 1 and 1.1. This is consistent with the results in section IV B where it is found that the nominal operating point is observed for a value of  $\theta$  higher than the design value.

The flow-rate range for which the static efficiency lays in the range  $60\% \leq \eta_s \leq 65\%$  is:  $2750 \lesssim Q \lesssim 4150 \text{ m}^3 \cdot \text{h}^{-1}$ , that is from 76% of the nominal flow-rate up to 115% of the nominal flow-rate. One open question is to what extent the global performances of the CRS are affected by the axial spacing and the speed ratio, and whether the efficient range could be extended by varying the speed ratio.

## B. Influence of the rotation ratio $\theta$

In this paragraph, the rotation rate of FR is kept constant at  $N_{FR} = 2000 \text{ rpm}$ , and the rotation rate of RR is varied from 0 rpm to 2400 rpm. The corresponding  $\theta$  are  $\theta = \{0; 0.5; 0.8; 0.85; 0.9; 0.95; 1; 1.05; 1.1; 1.15; 1.2\}$ . The axial spacing is  $S = 10 \text{ mm}$ .

The overall performances of the CRS in these conditions are plotted in Fig. 5. As expected, the more the rotation rate of RR increases, the more the static pressure rise of the CRS increases and the nominal flow-rate

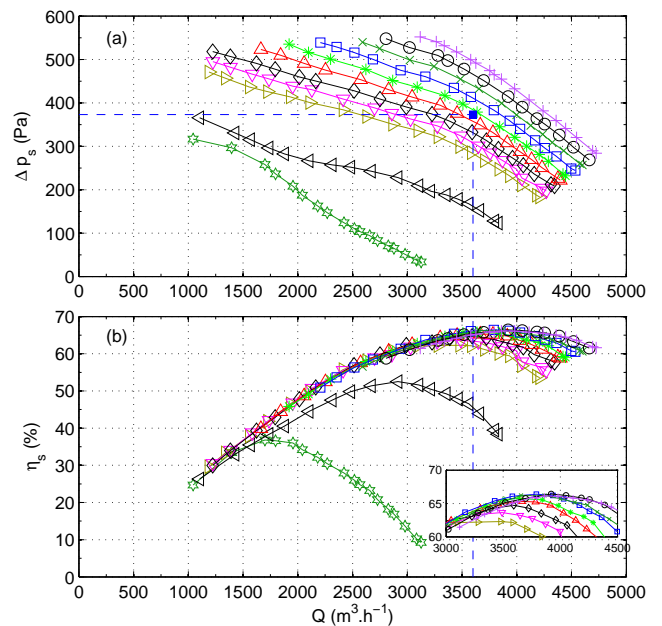


FIG. 5. CRS characteristics at  $N_{FR} = 2000 \text{ rpm}$ ,  $S = 10 \text{ mm}$  and  $\theta \in [0; 1.2]$ : (a) static pressure rise  $\Delta p_s$  vs flow rate  $Q$ ; (b) static efficiency  $\eta_s$  vs flow rate  $Q$ . Dark green  $\star$ :  $\theta = 0$ ; black  $\triangleleft$ :  $\theta = 0.5$ ; mustard yellow  $\triangleright$ :  $\theta = 0.8$ ; magenta  $\nabla$ :  $\theta = 0.85$ ; cyan  $\circ$ :  $\theta = 0.9$ ; red  $\triangle$ :  $\theta = 0.95$ ; green  $*$ :  $\theta = 1$ ; blue  $\square$ :  $\theta = 1.05$ ; dark green  $\times$ :  $\theta = 1.1$ ; black  $\circ$ :  $\theta = 1.15$  and purple  $+$ :  $\theta = 1.2$ . The blue  $\blacksquare$  and the dashed lines stand for the design point of the CRS

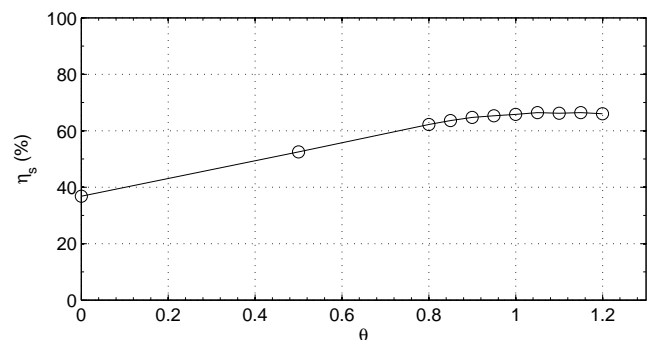


FIG. 6. Maximal static efficiency  $\eta_s$  vs  $\theta$  for the CRS with  $N_{FR} = 2000 \text{ rpm}$  and  $S = 10 \text{ mm}$

of the CRS increases. The maximal efficiency as a function of  $\theta$  is plotted in Fig. 6.

For very low rotation rates of RR, *i.e.* for  $\theta = 0$  (Dark green  $\star$  in Fig. 5) and  $\theta = 0.5$  (black  $\triangleleft$  in Fig. 5), the system is very inefficient: in the first case when the RR is at rest the maximum efficiency hardly reaches 35% which is below the maximal efficiencies of both FR and RR alone. The maximum flow-rate that can be reached is moreover very low in both cases compared to the discharge goal of  $3600 \text{ m}^3 \cdot \text{h}^{-1}$ .

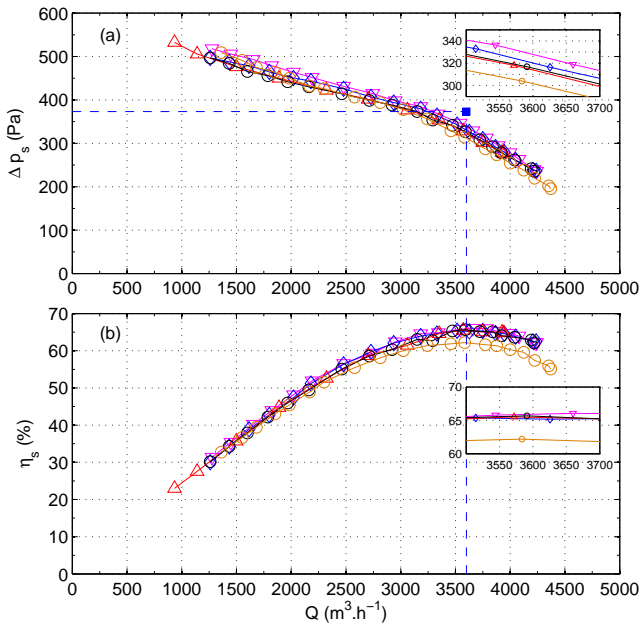


FIG. 7. CRS characteristics at various axial spacing: (a) static pressure rise  $\Delta p_s$  vs flow rate  $Q$ ; (b) static efficiency  $\eta_s$  vs flow rate  $Q$ . The rotation ratio of FR is  $N_{FR} = 2000 \text{ rpm}$  and  $\theta = 0.9$ . Magenta  $\nabla$ :  $S = 10 \text{ mm}$ , blue  $\circ$ :  $S = 20 \text{ mm}$ , red  $\triangle$ :  $S = 40 \text{ mm}$ , black  $\circ$ :  $S = 50 \text{ mm}$ , orange  $\times$ :  $S = 150 \text{ mm}$ . The blue  $\blacksquare$  and the dashed lines stand for the design point of the CRS

In the range  $\theta \in [0.8; 1.2]$ , *i.e.*  $N_{RR} \in [1600; 2400] \text{ rpm}$ , the system is highly efficient. The maximum efficiency increases with  $\theta$  to reach a maximum value of 66.5% for  $\theta = 1.05$  and is then quasi-constant ( $\eta_s = 66.0\%$  for  $\theta = 1.20$ ).

This is a very interesting feature of the counter-rotating system. One could imagine, simply by varying the rear rotor rotation rate, to work at a constant pressure rise with an efficiency greater than 60% for a large flow-rate range. For instance in the present case, the system could give a constant static pressure rise of 375 Pa with  $\eta_s \geq 60\%$  for  $3000 \leq Q \leq 4250 \text{ m}^3 \cdot \text{h}^{-1}$  with  $N_{FR} = 2000 \text{ rpm}$ ,  $S = 10 \text{ mm}$  and  $\theta \in [0.85; 1.2]$ .

One could also imagine to work at a constant flow-rate with high static efficiency. For instance in the present case, the system could give a constant flow-rate of  $3600 \text{ m}^3 \cdot \text{h}^{-1}$  with  $\eta_s \geq 60\%$  for  $290 \leq \Delta p_s \leq 490 \text{ Pa}$  with  $N_{FR} = 2000 \text{ rpm}$ ,  $S = 10 \text{ mm}$  and  $\theta \in [0.8; 1.2]$ .

### C. Influence of the axial spacing $S$

Five axial spacings were studied:  $S = 10, 20, 40, 50, \& 150 \text{ mm}$ . Before examining the axial spacing effect, let us take as a significant length scale the mean chord length of the front rotor ( $c_{FR} = 58 \text{ mm}$ ). We introduce the relative axial spacing  $A$ :

$$A = \frac{S}{c_{FR}} \quad (11)$$

The results reported here therefore concern  $A \in [0.17, 0.34, 0.69, 0.86, 2.58]$ .

Figure 7 shows the characteristics curves at the design rotation rates, *i.e.*,  $N_{FR} = 2000 \text{ rpm}$  and  $\theta = 0.9$ . Regarding  $A \in [0.17, 0.34, 0.69, 0.86]$ , the overall performances do not vary a lot. There is a slight tendency to a decrease in performance with increasing distances: at the design flow-rate, the difference in static pressure between the best case ( $S = 10 \text{ mm}$ ) and the worst case ( $S = 40 \text{ mm}$ ) is 17 Pa, which corresponds to a relative decrease of 5%. The efficiency does not vary significantly either.

In other studies<sup>3,4</sup> it was reported that the axial spacing had a more significant influence on the overall performances. This was noticed as well in this study. The orange curve in figure 7 shows that the performance when  $S = 150 \text{ mm}$  ( $A = 2.58$ ) is decreased by 28 Pa (8%) comparing to the other spacings. However, even for  $S = 150 \text{ mm}$ , the CRS still shows good performances with high efficiency compared to the conventional fan systems. In section V, measurements of the wall pressure fluctuations shows that increasing the axial spacing to a certain extent (*i.e.* that keeps good performances), has the advantage of reducing the rotors interaction and a priori reducing the surrounding noise.

## V. WALL PRESSURE FLUCTUATION MEASUREMENTS

The wall pressure fluctuations were recorded for two axial spacings:  $S = \{10; 150\}$ . For both configurations, four microphones were regularly spaced around the duct circumference (90 spacing) and 5 mm downstream the front rotor. The signal is sampled at  $f_s = 6000 \text{ Hz}$  for  $t = 20 \text{ s}$ . Figure 8 shows the power spectral density for  $S = 10 \text{ mm}$  (blue curve) and  $S = 150 \text{ mm}$  (red curve).

One can see that the blue curve has much more frequency components than the red curve. Among those frequency peaks, there are the blade passing frequency (and its harmonics) of the front rotor:  $f_{bpFR} = 11 \times 2000 / 60 = 366.7 \text{ Hz}$  and the blade passing frequency (and its harmonics) of the rear rotor:  $f_{bpRR} = 7 \times 1800 / 60 = 210 \text{ Hz}$ . Please notice that  $f_{bpFR}$  peaks of the blue curve are hidden by those of the red curve. The peaks of the rear rotor blade passing frequencies are much higher than those of the front rotor despite the fact that the rear rotor rotation ratio is lower than the front rotor rotation ratio. This is consistent with the fact that the RR has less blades than the FR and performs more pressure rise than the FR alone (assuming that the FR does the same pressure rise with and without the RR). The RR's blades are therefore more loaded which results in higher peak levels as can be observed

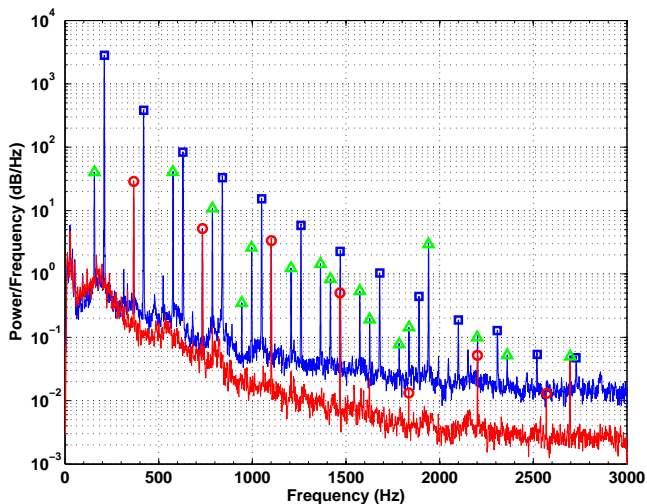


FIG. 8. Power spectral density of the wall pressure fluctuations 5 mm downstream the front rotor. The signal is sampled at  $f_s=6000$  Hz for  $t=10$  s. The blue curve stands for the axial spacing  $S=10$  mm and the red curve for  $S=150$  mm. The red  $\circ$  and blue  $\square$  stand for the blade passing frequencies of the front rotor and the rear rotor, respectively. The green  $\triangle$  are the rotors interaction peaks.

on Fig 8. Moreover, along the blade passing frequencies new frequencies appear corresponding to the rotors interaction and are equal to:

$$f = m * f_{bpFR} + n * f_{bpRR} \quad (12)$$

where  $m$  and  $n$  are integer.

Figure 9 graphs the autocorrelation coefficients of the microphone number 2 (blue curve) and the cross-correlation between microphone number 1 and 2 (green curve) for  $S=10$  mm. The rear rotor rotation direction is from microphone one to microphone two. The abscissa axis represents the rear rotor rotation (dimless). That is e.g., from 0 to 1 corresponds to one revolution of the rear rotor.

Both curves are periodic and highly correlated. One can count seven periods for the autocorrelation curve for one revolution and that is the number of blade of the rear rotor. Furthermore, the period  $t_1=4.833$  ms corresponds to  $f_1=210$  Hz. Again, this is the blade passing frequency of the rear rotor,  $f_{bpRR}$ . According to the cross-correlation curve, the flow structure near by the microphone number one is very similar to that of the microphone number two. The green curve is shifted by  $t_2=t_1/4$  and that is the time to go from microphone one to microphone two. This observation could mean that there is a coherent structure located at least in the tip region and travelling at the same rotation ratio of the rear rotor and in the same direction. All these remarks lead to think that the rear rotor generates and impose its frequency to the flow structure in the inter-rotors region.

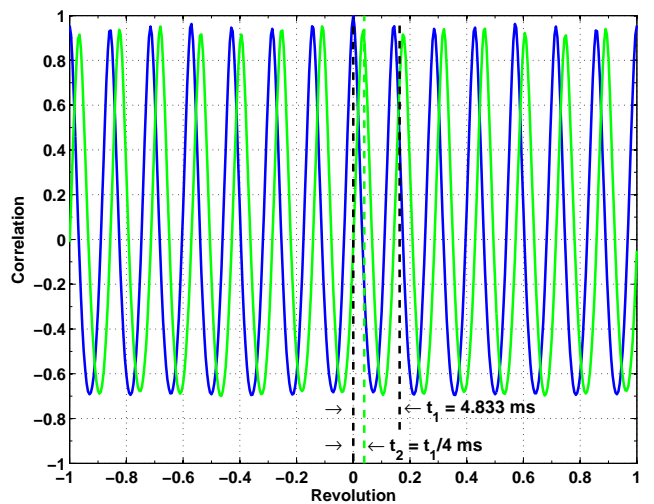


FIG. 9. Correlation coefficients of the wall pressure fluctuations at  $S=10$  mm. The time on the abscissa axis is made dimensionless, i.e.,  $t' = t * f_{RR}$  and represents two revolutions of the rear rotor. The blue curve stands for the autocorrelation coefficients of the microphone 2. The green curve stands for the cross-correlation of the microphones 1 and 2.  $t_1$  and  $t_2$  are the periods of the blue curve and the green curve respectively.

Let us consider the case where  $S=150$  mm. Recall that the microphones are still 5 mm downstream the front rotor and thus 145 mm upstream the rear rotor. Its power spectral density in figure 8 (red curve) shows only the blade passing frequencies of the front rotor. The blade passing frequencies of the rear rotor do not appear any more. The peaks level are noticeably the same. In the same way, the autocorrelation coefficients of the microphone number 2, red curve on figure 10, are very low for  $S=150$  mm. One can count eleven periods on the red curve, and that is the number of blade of the front rotor and the period  $t_3=2.7$  ms corresponds to  $f_3=370.4$  Hz which is very near to the front rotor blade passing frequency. It is clear from above that the interaction between rotors tends to decrease when increasing the axial spacing, at least, the FR does not see the influence of the RR. On the other hand, it does not mean that the RR does not contribute to the whole noise emission or that the rotors interaction does not exist anymore when the axial spacing is increased.

## VI. CONCLUSION

A counter-rotating axial-flow fan has been designed according to an iterative method that is relatively fast. It is based on semi-empirical modelization that partly takes into account the losses, boundary layers at hub and casing, and the effects of “low” Reynolds numbers (below  $2 \times 10^5$ ).

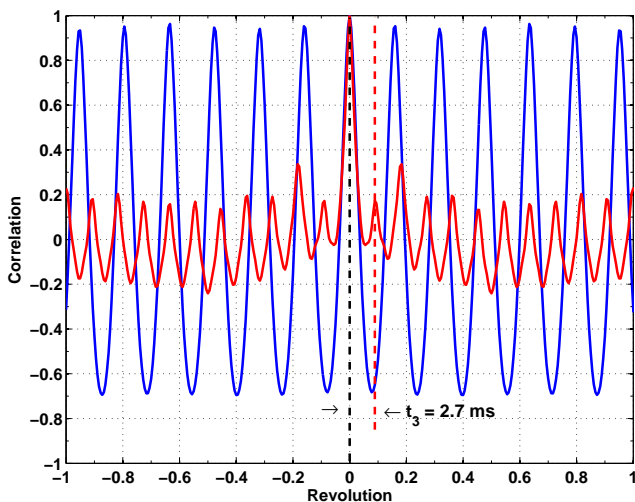


FIG. 10. Correlation coefficients of the wall pressure fluctuations. The time on the abscissa axis is made dimensionless, i.e.,  $t' = t * f_{FR}$  and represents two revolutions of the front rotor. The blue curve stands for the autocorrelation coefficients of the microphone 2 at  $S=10$  mm whereas the red curve stands for autocorrelation of the microphones 2 at  $S=150$  mm.  $t_3$  is the period of the red curve.

The overall performances at the nominal design point are slightly lower than predicted, with a static pressure rise 10.2% lower. The static efficiency is however remarkably high ( $\eta_s \simeq 65\%$ ) and corresponds to a 20 points gain in efficiency with respect to the front rotor maximal efficiency and to a 10 points gain with respect to the rear rotor. The overall measurements give first clues that allow to validate the design method.

The counter-rotating system has a very flexible use that allows to work at constant flow-rate on a wide range of static pressure rises or to work at constant pressure rise on a wide range of flow-rates, with static efficiency bigger than 60%, simply by varying the Rear Rotor rotation rate. One could thus imagine an efficient closed-loop-controlled axial-flow fan. The overall performances moreover do not significantly vary with the axial spacing in the range  $A \in [0.17; 0.86]$ . However, for  $A = 2.58$  the overall performances slightly decrease.

The wall pressure fluctuations investigation, which is representative of the very near-field noise emission, shows a strong influence of the rear rotor over the flow structure between rotors when they are close to each other. But increasing  $A$  leads to only remove the rotors interaction near by the FR without decreasing a lot the overall performances. These results is encouraging to study deeper the effect of the axial spacing on the noise emission on the far-field.

Local measurements of the velocity field in the wake of the front rotor rotating alone are scheduled, in order to confirm the design. These measurements will also be of great interest concerning the understanding of the inter-

action in the space between the rotors.

## ACKNOWLEDGMENT

The authors finally wish to thank Robert Rey for very fruitful discussions.

## NOMENCLATURE

$\alpha$	Flow angle in the absolute reference frame.
$\beta$	Flow angle in the relative reference frame.
$\mathcal{D}$	Lieblein's diffusion factor.
$\Delta p$	Pressure rise.
$\eta$	Efficiency.
$\gamma$	Stagger angle.
$\Omega$	Specific speed.
$\omega$	Angular velocity.
$\phi$	Flow coefficient.
$\psi$	Pressure coefficient.
$\rho$	Density.
$\sigma$	Blade solidity.
$\theta$	Rotation ratio $\frac{N_{RR}}{N_{FR}}$ .
1	Fan inlet
2	Fan outlet
A	Relative axial spacing, $S/c$ .
a	Angle of attack.
a	Axial
C	Flow velocity in the absolute reference frame.
c	Chord length.
$C_{z\infty 0}$	Camber coefficient.
CRS	Counter-rotating system.
D	Ducting pipe diameter.
$e\%$	Relative thickness.
est	Estimate
FR	Front rotor.
m	Mean
N	Rotation rate.

Q	Flow rate.
R	Blade radius.
r	Radial
RR	Rear rotor.
S	Axial spacing.
s	Static
T	Torque supplied by the shaft.
t	Total
U	Moving frame speed.
u	Tangential
W	Flow velocity in the relative reference frame.
x/c	Relative chord wise location.
Z	Number of blades.

## BIBLIOGRAPHY

- <sup>1</sup>Lesley, E., 1933. Experiments with a counter-propeller. Tech. Rep. 453, National Advisory Committee for Aeronautics.
- <sup>2</sup>Lesley, E., 1939. Tandem air propellers. Tech. Rep. 689, National Advisory Committee for Aeronautics.
- <sup>3</sup>Sharma, P., Jain, Y., and Pundhir, D., 1988. "A study of some factors affecting the performance of a contra-rotating axial compressor stage". *Proceedings of the Institution of Mechanical Engineers. Part A. Power and process engineering*, **202**, pp. 15–21.
- <sup>4</sup>Sharma, P., Pundhir, D., and Chaudhry, K., 1991. "A study of aeroacoustic performance of a contra-rotating axial flow compressor stage". *Def Sci J*, **41**, pp. 165–180.
- <sup>5</sup>Min, K.-S., Chang, B.-J., and Seo, H.-W., 2009. "Study on the contra-rotating propeller system design and full-scale performance prediction method". *International Journal of Naval Architecture and Ocean Engineering*, **1**, pp. 29–38.
- <sup>6</sup>Shigemitsu, T., Furukawa, A., Watanabe, S., Okuma, K., and Fukutomi, J., 2009. "Internal flow measurement with ldv at design point of contra-rotating axial flow pump". *Journal of Fluid Science and Technology*, **4**, pp. 723–734.
- <sup>7</sup>Shigemitsu, T., Fukutomi, J., and Okabe, Y., 2010. "Performance and flow condition of small-sized axial fan and adoption of contra-rotating rotors". *Journal of Thermal Science*, **19**, pp. 1–6.
- <sup>8</sup>Shigemitsu, A., Watanabe, T., and Furukawa, S., 2007. "Performance test and flow measurement of contra-rotating axial flow pump". *Journal of Thermal Science*, **16**(1), pp. 7–13.
- <sup>9</sup>Pin, L., Yingzi, J., and Yanping, W., 2011. "Effects of rotors structure on performance of small size axial flow fans". *Journal of Thermal Science*, **20**, pp. 205–210.
- <sup>10</sup>Noguera, R., Rey, R., Massouh, F., Bakir, F., and Koudri, S., 1993. "Design and analysis of axial pumps". In ASME Fluids Engineering, Second Pumping Machinery Symposium, Washington, USA., pp. 95–111.
- <sup>11</sup>Lieblein, S., Schwenk, F. C., and Broderick, R. L., 1953. Diffusion factor for estimating losses and limiting blade loading in axial-flow-compressor blade elements. Tech. Rep. TM E53D01, National Advisory Committee for Aeronautics.
- <sup>12</sup>ISO, 2007. *ISO 5801 - Industrial fans Performance testing using standardized airways*. International Standards for Business, Government and Society.
- <sup>13</sup>Sarraf, C., Nouri, H., Ravelet, F., and Bakir, F., 2011. "Experimental study of blade thickness effects on the global and local performances of a controlled vortex designed axial-flow fan". *Experimental Thermal and Fluid Science*, **35**, p. 684.
- <sup>14</sup>Moreau, S., and Bakir, F., 2002. "Efficient stator designed for automotive engine cooling fan systems". In ASME 2002 Fluids Engineering Division Summer Meeting, pp. FEDSM02–31318.
- <sup>15</sup>Bakir, F., and Moreau, S., 2003. "Detailed study of an efficient small diameter automotive engine cooling fan system". In ASME 2003 Fluids Engineering Division Summer Meeting, pp. FEDSM2003–45117.